Some applications of a two-fluid model

Fabien Crouzet, Frédéric Daude, Pascal Galon, Jean-Marc Hérard, Olivier Hurisse, Yujie Liu

Some applications of a two-fluid model

Fabien Crouzet, Frédéric Daude, Pascal Galon, Jean-Marc Hérard, Olivier Hurisse, Yujie Liu

Abstract We present in this paper some comparisons of numerical results and experimental data in some two-phase flows involving rather high pressure ratios. A two-fluid two-phase flow model has been used herein, but we also report a few results obtained with some simpler single-fluid two-phase flow models.

1 Introduction

The correct modelling of two-phase flows still requires a further investigation of models and methods, but also demands more details and a thorough comparison with available experimental data. For most of the water-vapour applications arising within the framework of nuclear power plants, the vapour phase is dilute ; however, the mean flow may sometimes contain a much larger amount of vapour (this may occur in the upper part of steam generators, or more likely in some severe accident configurations following the boiling crisis, or in water-hammer situations), and thus relative velocities may become large. This, among other reasons, has motivated the focus on a class of two-fluid models for which the numerical simulation of highly unsteady flows is relevant. Actually, when restricting to the statistical averaging formalism, we know that standard tools may be used in order to derive meaningful models, in order to tackle unsteady and inhomogeneous two-phase flow patterns.

The two-fluid two-phase flow model discussed herein belongs to a wider class that has been investigated in [3, 17, 11, 4, 10, 8, 16] among other references. It re-

Fabien Crouzet, Frédéric Daude, Yujie Liu: EDF R&D, AMA, and LAMSID, UMR EDF/ CNRS/ CEA 2832, 1 avenue du Général de Gaulle, F-92141 Clamart (fabien.crouzet@edf.fr, frederic.daude@edf.fr, yujie.liu@edf.fr)
Pascal Galon: CEA Saclay, Gif sur Yvette (pascal.galon@cea.fr)
Jean-Marc Hérard, Olivier Hurisse: EDF R&D, MFEE, 6 quai Watier, F-78400 Chatou (jean-marc.herard@edf.fr,olivier.hurisse@edf.fr)

quires the computation of seven unknowns (statistical void fraction of the vapour, mean densities, mean velocities and mean pressures). As recalled in [7, 15] for instance, partial differential equations may be derived for statistical void fractions, and partial mass, momentum and total energy within each phase ; equations of state which provide the mean internal energy within each phase must be prescribed, and some other closure laws for cross-correlations and interfacial transfer terms are also necessary.

We recall in section 2 the governing equations and their main properties ; afterwards we briefly describe the basics of the Finite Volume scheme that is used for numerical simulations. Then we focus on the main part, which consists in reporting some numerical results that have been obtained in [18], thus including a comparison with experimental data [19, 21], but also with other numerical results.

2 Governing equations

Classical notations are used, hence $\alpha_k(x,t)$ will denote the statistical void fraction of phase $k = l, v$, and will comply with the constraint $\alpha_l(x,t) + \alpha_v(x,t) = 1$. Variables ρ_k, U_k, P_k respectively denote the mean density, the mean velocity, the mean pressure within phase k, and we define partial masses $m_k = \alpha_k \rho_k$. The total energy E_k within phase $k = l, v$ is defined by: $E_k = \rho_k e_k(P_k, \rho_k) + \rho_k (U_k^2)/2$, where $e_k(P_k, \rho_k)$ stands for the internal energy. The state variable W will be noted:

$$W^t = (\alpha_v, m_l, m_v, m_l U_l, m_v U_v, \alpha_l E_l, \alpha_v E_v)$$

Thus, when neglecting the contribution of viscous effects and turbulence, the form of the governing equations of mean quantities in the two-fluid model is, for $k = l, v$:

$$\begin{array}{l}
\partial_t(\alpha_v) + V_{int}(W)\partial_x(\alpha_v) = \phi_v(W) \\
\partial_t(m_k) + \partial_x(m_k U_k) = \Gamma_k(W) \\
\partial_t(m_k U_k) + \partial_x\left(m_k U_k^2\right) + \partial_x(\alpha_k P_k) - \Pi_{int}(W)\partial_x(\alpha_k) = D_k(W) + \Gamma_k(W)\overline{U}_{int} \\
\partial_t(\alpha_k E_k) + \partial_x(\alpha_k U_k(E_k + P_k)) + \Pi_{int}(W)\partial_t(\alpha_k) = \psi_k(W) + \overline{U}_{int} D_k(W) + \Gamma_k(W)\overline{H}_{int}
\end{array} \tag{1}$$

Contributions $\Gamma_k(W)$, $D_k(W)$ and $\psi_k(W)$ take interfacial mass transfer, drag effects and interfacial heat transfer into account. Besides, the term $\phi_k(W)$ arising in the governing equation of the statistical void fraction α_k is due to the statistical averaging ([7, 15]) of the topological equation. The following constraints also hold:

$$\sum_{k=l,v} \Gamma_k(W) = 0 \quad ; \quad \sum_{k=l,v} \psi_k(W) = 0 \quad ; \quad \sum_{k=l,v} D_k(W) = 0 \quad ; \quad \sum_{k=l,v} \phi_k(W) = 0 \, . \tag{2}$$

and we define: $\overline{U}_{int} = (U_l + U_v)/2$ and: $\overline{H}_{int} = U_l U_v/2$. Furthermore, we define $V_{int}(W)$ as:

$$V_{int}(W) = \xi(W) U_l + (1 - \xi(W)) U_v \, . \tag{3}$$

where $\xi(W)$ lies in $[0,1]$. Physically relevant functions $\xi(W)$ have been proposed in [8], and will be recalled at the end of this section. We also introduce the specific entropy $S_k(P_k,\rho_k)$ in each phase, which complies with:

$$c_k^2 \partial_{P_k}(S_k) + \partial_{\rho_k}(S_k) = 0 \tag{4}$$

-noting $c_k(W)$ the speed of acoustic waves within phase k- and temperatures: $1/T_k = \partial_{P_k}(S_k)/\partial_{P_k}(e_k)$; we also set: $\mu_k = e_k + P_k/\rho_k - T_k S_k$. Besides, source terms $\Gamma_l(W), \phi_l(W), \psi_l(W), D_l(W)$ are defined as (see property 1):

$$\begin{array}{rrcrr} \Gamma_l(W) = & K_\Gamma(W)(\mu_v(W)/T_v - \mu_l(W)/T_l) & ; & D_l(W) = & K_U(W)(U_v - U_l)\,; \\ \psi_l(W) = & K_T(W)(T_v - T_l) & ; & \phi_l(W) = & K_P(W)(P_l - P_v) \end{array}$$

The first three closure laws were expected, and the last one is physically relevant: it simply means that the statistical void fraction of the liquid phase locally increases when $P_l > P_v$. The -positive- scalar functions in the drag contribution and in the heat transfer closure law may be chosen as:

$$K_U(W) = m_l m_v/(m_l+m_v)/\tau_U(W),$$

$$K_T(W) = m_l m_v C_{l-v}/(m_l+m_v)/\tau_T(W),$$

$$K_P(W) = \alpha_l \alpha_v/(P_l+P_v)/\tau_P(W).$$

Here, $\tau_{U,P,T}(W)$ denote velocity-pressure-temperature relaxation time scales, and we also set : $K_\Gamma(W) = K'_\Gamma(W)/\tau_\Gamma(W)$. Closure laws for $\tau_{U,P,T,\Gamma}(W)$ can be found in the literature (see [9] for a review concerning τ_P). Eventually, we assume that $\Pi_{int}(W)$ is a convex combination of both pressures, thus:

$$\Pi_{int}(W) = \chi(W) P_l + (1-\chi(W)) P_v \tag{5}$$

with:

$$\chi(W) = (1-\xi(W))/T_l((1-\xi(W))/T_l + \xi(W)/T_v)^{-1} \tag{6}$$

Property 1:
For smooth solutions W of (1) *with closure laws* (3), (5), (6)*, the governing equation of the entropy of the two-fluid model* $\eta(W) = \sum_{k=l,v} m_k S_k$ *is:*

$$\begin{aligned} \partial_t(\eta(W)) + \partial_x\left(\sum_{k=l,v} m_k U_k S_k\right) = & \quad \Gamma_l(W)(\mu_v(W)/T_v - \mu_l(W)/T_l) \\ & + D_l(W)(U_v - U_l)(1/(2T_v) + 1/(2T_l)) \\ & + \psi_l(W)(T_v - T_l)/(T_v T_l) \\ & + \phi_l(W)(P_l - P_v)((1-\chi(W))/T_v + \chi(W)/T_l) \end{aligned}$$

Obviously, when $\xi(W)=0$ (or $\xi(W)=1$), one retrieves the standard Baer-Nunziato model [3], where the interface velocity $V_{int}(W)$ corresponds to the mean velocity of the vanishing phase ([3, 17, 4] and [10] also). We finally recall two basic properties:

- **Property 2:** *The set of equations associated with the left-hand side of* (1) *has seven real eigenvalues which read:*

$$\lambda_1 = V_{int}(W) \tag{7}$$

$$\lambda_2 = U_v, \quad \lambda_3 = U_v - c_v(W), \quad \lambda_4 = U_v + c_v(W), \tag{8}$$

$$\lambda_5 = U_l, \quad \lambda_6 = U_l - c_l(W), \quad \lambda_7 = U_l + c_l(W) \tag{9}$$

  Associated righteigenvectors span the whole space $\mathscr{R}^7$, if: $|U_k - V_{int}(W)|/c_k \neq 1$.

- **Property 3:** *Fields associated with eigenvalues $\lambda_{2,5}$ are linearly degenerate. Other fields associated with eigenvalues $\lambda_{3,4,6,7}$ are non linear. The $1-$field is linearly degenerate if: $\xi(W)(1-\xi(W))=0$, or if: $\xi(W)=m_l/(m_l+m_v)$.*

If the 1-field is linearly degenerate, unique jump conditions can be written within each single field. Thus, for suitable schemes that provide convergent schemes when the mesh is refined, we expect that approximations converge towards the unique shock solution. Other properties can be found in [5].

3 Finite Volume scheme

The basic algorithm that is used to compute approximations of the whole system relies on an entropy-consistent fractional step method including an evolution step and a relaxation step. Details on schemes can be found in references [8, 12, 13, 14].

- *Evolution step*
  This step computes approximate solutions of the homogeneous system:

$$\begin{cases} \partial_t(\alpha_v) + V_{int}(W)\partial_x(\alpha_v) = 0 \\ \partial_t(m_k) + \partial_x(m_k U_k) = 0 \\ \partial_t(m_k U_k) + \partial_x\left(m_k U_k^2\right) + \partial_x(\alpha_k P_k) - \Pi_{int}(W)\partial_x(\alpha_k) = 0 \\ \partial_t(\alpha_k E_k) + \partial_x(\alpha_k U_k(E_k+P_k)) + \Pi_{int}(W)\partial_t(\alpha_k) = 0 \end{cases} \tag{10}$$

  through the time interval $[t^n, t^n+\Delta t]$, with given initial values W^n. The Finite Volume solver that is used to compute interface fluxes either relies on a non-conservative version of the Rusanov scheme, on the approximate VFRoe-ncv Godunov scheme (see [8]), or on the relaxation scheme introduced in [20] (see [1, 2] too). An explicit CFL condition enforces the time step. This provides a set of approximations $\tilde{W}$. An extensive verification of convective schemes can be found in [6], with focus on solutions on one-dimensional Riemann problems.

- *Relaxation step*
  Given discrete cell values of $\tilde{W}$, we compute approximations of the coupled set of ODEs corresponding to relaxation terms, that is:

$$\begin{cases} \partial_t(\alpha_v) = \phi_v(W) \\ \partial_t(m_k) = \Gamma_k(W) \\ \partial_t(m_k U_k) = D_k(W) + \Gamma_k(W)\overline{U}_{int} \\ \partial_t(\alpha_k E_k) + \Pi_{int}(W)\partial_t(\alpha_k) = \psi_k(W) + \overline{U}_{int} D_k(W) + \Gamma_k(W)\overline{H}_{int} \end{cases} \tag{11}$$

  The most difficult task in the building of the Finite Volume solver is due to the mass transfer term and to the contribution ϕ_k. In particular, difficulties arise when enforcing the conservative form for the mixture, and meanwhile requesting that void fractions and pressures should remain in their physical range. Many details on this part of the algorithm can be found in [12, 13, 14].

4 A comparison of computational results with experimental data

We provide numerical results and a comparison with experimental data for two distinct cases characterized by high pressure variations.

Simpson experiment This experiment is described in [21]. A big tank is filled with water that flows in a small pipe, the diameter of which is 19 mm; at the very beginning of the recording, the velocity of the fluid is equal to 0.4 m/s, the pressure in the tank is $3.419 \times 10^5 Pa$, the temperature is $T = 296$ K. The pipe of 36 meters length is suddenly closed at its right end; thus it results in a violent water-hammer. A shock wave is created and propagates to the left towards the tank. Three pressure captors have been inserted along the pipe, and focus is given here on the one that is close to the right closed exit. The one-dimensional mesh in the pipe contains 12000 regular cells, and the CFL has been set to $1/2$. Numerical results obtained with a finer mesh with 36000 cells differ from the latter of less than one percent. A stiffened gas equation of state (EOS) has been used in the liquid phase, whereas a perfect gas EOS is retained for the vapour phase. In figure 1, the time evolution of the mean pressure $P = \alpha_v P_v + (1-\alpha_v)P_l$ for this captor has been displayed (orange squares), and a comparison with numerical results obtained with the two-fluid approach on the fine mesh can be done (light blue line). The red triangles refer to the two-fluid approach when one accounts for the elasticity of the pipe (see [18]). Obviously, the prediction of maximum and mimimum values in the transient, as well as occurences of sudden increases and decreases, highly depends on the elasticity of the pipe, and whether it has been accounted for or not in the whole model. This pattern is even emphasized in some other experiments (for instance in Romander experiment, where a wave propagates in a pipe including a rigid section and an elasto-plastic section, see [18]).

.

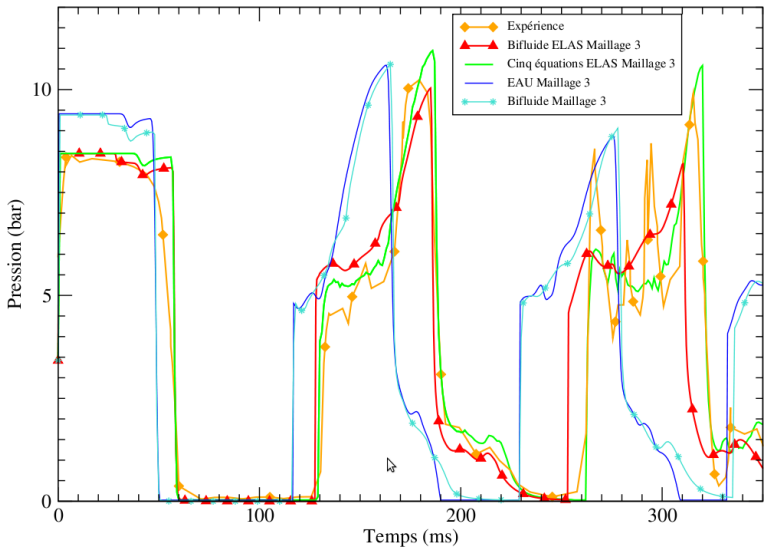

Fig. 1 Time evolution of the pressure $P = \alpha_v P_v + (1-\alpha_v)P_l$ in Simpson experiment (orange squares). Numerical results: Red triangles - two-fluid model with fluid-structure interaction / Green line - five-equation homogeneous model with fluid-structure interaction / Light blue line - two-fluid model without fluid-structure interaction / Dark blue line - three-equation homogeneous model without fluid-structure interaction.

Canon experiment In this second experiment [19], a closed rigid pipe initially filled with pressurized water is suddenly opened at its right end. This results in a sudden vaporisation of the fluid, and a left-going rarefaction wave is propagating in the liquid region. The initial pressure $P = \alpha_v P_v + (1-\alpha_v)P_l$ in the pipe is $32 \times 10^5 Pa$, the initial uniform temperature is $T_v = T_l = 493$ K, and the fluid ($\alpha_v = 10^{-3}$) is at rest: $U_v = U_l = 0$. The same EOS have been used within the liquid and vapour phases for this second experiment, and the time step is still chosen in agreement with the constraint: $CFL = 1/2$. The mesh for which results are displayed contains 8000 cells along the pipe axis. Several data have been collected, and results presented in figure 2 (black squares) correspond to the time evolution of the pressure close to the right end. A sudden decrease can be oberved first, followed by an almost contant state corresponding to the saturation pressure; afterwards a second smooth decrease occurs, together with an intense vaporization (see figure 3), until the atmospheric pressure is reached. Vapour statistical fractions have been recorded at the same place as time goes on, for different experimental runs (orange crosses in figure 3). Numerical results obtained with the two-fluid model on a fine mesh have been plotted on both figures 2-3, together with approximations provided by two different homogeneous models (a five-equation model and a three-equation model). Obviously the vaporization occurs sooner in the simulation than in the experiment.

.

.

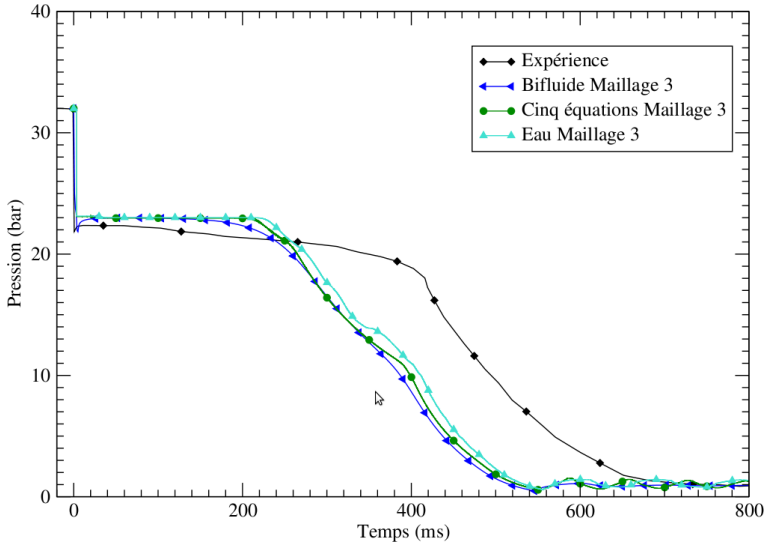

Fig. 2 Time evolution of the pressure $P = \alpha_v P_v + (1-\alpha_v)P_l$ in Canon experiment (black squares). Numerical results: Dark blue: two-fluid model / Green: five-equation homogeneous model / Light blue: three-equation homogeneous model.

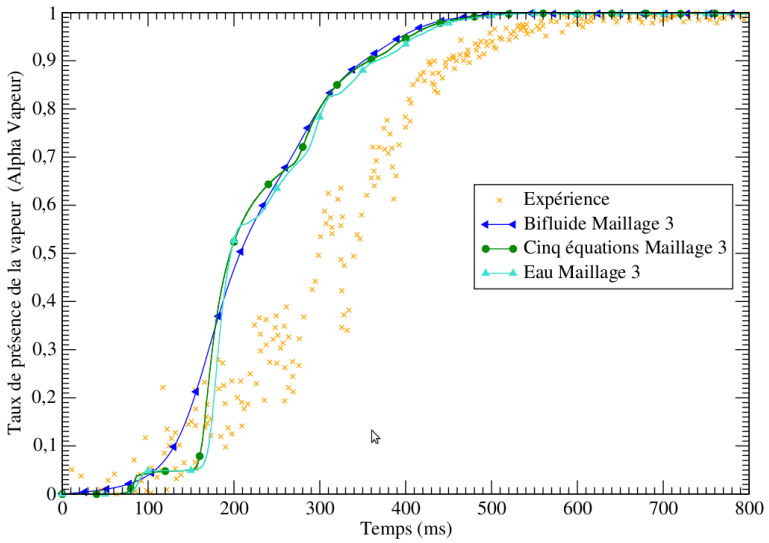

Fig. 3 Time evolution of the vapour statistical fraction in Canon experiment (orange crosses for different runs). Numerical results: Dark blue triangles - two-fluid model / Green dots - five-equation homogeneous model / Light blue: three-equation homogeneous model.

Acknowledgements The last author received a financial support by ANRT through an EDF-CIFRE contract 732/2010. Computational facilities were provided by EDF. Numerical simulations have been performed with the Europlexus code.

References

1. A. Ambroso, C. Chalons, F. Coquel, T. Galié, Relaxation and numerical approximation of a two-fluid two-pressure diphasic model. ESAIM: M2AN, **43 (6)**, pp. 1063–1097 (2009).
2. A. Ambroso, C. Chalons, P.A. Raviart, A Godunov-type method for the seven-equation model of compressible two-phase flow. Computers and Fluids, **54**, 67-91.(2012)
3. M.R. Baer, J.W. Nunziato, A two-phase mixture theory for the deflagration to detonation transition (DDT) in reactive granular materials, IJMF, **12(6)**, pp. 861-889, (1986).
4. J.B. Bdzil, R. Menikoff, S.F. Son, A.K. Kapila, D.S. Stewart, Two phase modelling of deflagration to detonation transition in granular materials: a critical examination of modelling issues, Phys. of Fluids, **11**, pp. 378–402, (1999).
5. F. Coquel, J.M. Hérard, K. Saleh, N. Seguin, Two properties of two-velocity two-pressure models of two-phase flows, Communications in Mathematical Sciences, **12(3)**, pp. 593-600 (2014).
6. F. Crouzet, F. Daude, P. Galon, P. Helluy, J.M. Hérard, O. Hurisse, Y. Liu, Approximate solutions of the Baer Nunziato model, ESAIM proceedings, **40**, pp. 63-82 (2013)
7. D.A. Drew, S.L. Passman, Theory of multi-component fluids, Applied Mathematical Sciences, **135**, Springer, (1999).
8. T. Gallouët, J.M. Hérard, N. Seguin, Numerical modelling of two phase flows using the two-fluid two-pressure approach, Math. Mod. Meth. in Appl. Sci., **14(5)**, pp. 663-700, (2004).
9. S. Gavrilyuk, The structure of pressure relaxation terms: one-velocity case. preprint (2013).
10. S. Gavrilyuk, R. Saurel, Mathematical and numerical modelling of two-phase compressible flows with micro-inertia, J. Comp. Phys., **175**, pp. 326-360, (2002).
11. J. Glimm, D. Saltz, D.H. Sharp, Two-phase flow modelling of a fluid mixing layer, J. Fluid Mech., **378**, pp. 119–143, (1999).
12. J.M. Hérard, O. Hurisse, Schémas d'intégration du terme de relaxation des pressions phasiques pour un modèle bifluide hyperbolique, EDF report H-I81-2009-01514-FR, (2009).
13. J.M. Hérard, O. Hurisse, Computing two-fluid models of compressible two-phase flows with mass transfer, AIAA paper 2012-2959 (2012).
14. J.M. Hérard, O. Hurisse, A fractional step method to compute a class of compressible gas liquid flows. Computers and Fluids, **55**, 57-69. (2012).
15. J.M. Hérard, Y. Liu, Une approche bifluide statistique de modélisation des écoulements diphasiques à phases compressibles. EDF report H-I81-2013-01162-FR (2013).
16. M. Ishii, T. Hibiki, Thermofluid dynamics of two-phase flow, Springer, (2006).
17. A.K. Kapila, S.F. Son, J.B. Bdzil, R. Menikoff, D.S. Stewart, Two phase modeling of a DDT: structure of the velocity relaxation zone, Phys. of Fluids, **9(12)**, pp. 3885–3897, (1997).
18. Y. Liu, Contribution à la vérification et á la validation d'un modèle diphasique bifluide instationnaire. PhD thesis, Université Aix-Marseille, Marseille, France, 11/09/2013. http://tel.archives-ouvertes.fr/tel-00864567
19. B. Riegel, Contribution à l'étude de la décompression d'une capacité en régime diphasique. PhD thesis, Université de grenoble 1978.
20. K. Saleh, Analyse et Simulation Numérique par Relaxation d'Ecoulements Diphasiques Compressibles. Contribution au Traitement des Phases Evanescentes. PhD thesis, Université Pierre et Marie Curie, Paris, France, 26/11/2012. http://tel.archives-ouvertes.fr/tel-00761099
21. A.R. Simpson, Large water-hammer pressures due to column separation in sloping pipes (transient cavitation). PhD thesis, University of Michigan, 1986.